FOURTEENTH EUROPEAN ROTORCRAFT FORUM

Paper No. 13

COMPARISON WITH EXPERIMENT OF VARIOUS COMPUTATIONAL METHODS OF AIRFLOW ON THREE HELICOPTER FUSELAGES

S.R. Ahmed, J. Amtsberg
DFVLR, Braunschweig, W.-Germany

A.C. de Bruin
NLR, Amsterdam, The Netherlands

A. Cler
Aerospatiale, Marignane, France

G. Falempin, T.H. Le
ONERA, Chatillon, France

G. Polz
MBB, Ottobrunn/München, W.-Germany

F.T. Wilson
Westland Helicopters Ltd., Yeovil, England

September, 20-23, 1988
MILANO, ITALY

ASSOCIAZIONE INDUSTRIE AEROSPATIALI
ASSOCIAZIONI ITALIANA DI AERONAUTICA E ASTRONAUTICA

COMPARISON WITH EXPERIMENT OF VARIOUS COMPUTATIONAL METHODS OF AIRFLOW ON THREE HELICOPTER FUSELAGES

S.R. Ahmed, J. Amtsberg
DFVLR, Braunschweig, W.-Germany

A.C. de Bruin
NLR, Amsterdam, The Netherlands

A. Cler
Aerospatiale, Marignane, France

G. Falempin, T.H. Le
ONERA, Chatillon, France

G. Polz
MBB, Ottobrunn/München, W.-Germany

F.T. Wilson
Westland Helicopters Ltd., Yeovil, England

Abstract

Computational methods developed or in use at ONERA, Westland Helicopters Ltd., Aerospatiale and NLR have been applied to predict the surface pressure, rotor-plane velocity distribution and boundary layer development on three fuselage configurations which are typical of current generation of helicopters. Rotor flow was not simulated.

Basis for validation of the computer codes was an extensive experimental study by DFVLR, conducted with a 1:7-scale wind tunnel model with variable rear end. Configurations generated were streamline, upswept- and flat back rear-end helicopter fuselages.

1. Introduction

Aerodynamics of the helicopter fuselage and its interaction with main and tail rotor can have a dramatic effect on the performance of high speed helicopters. Reduction of drag and vibration, increase in flight speed, fuel efficiency, and better flying qualities etc. are the payoff resulting from improved fuselage aerodynamics.

The fuselage of a helicopter underlies operational requirements which impose unfavourable geometric constraints on the afterbody geometry. The bluff aft-fuselage creates an extensive region of separation in the rear, leading to a large amount of pressure drag. An upswept rear-end, unfavourably designed, generates strong longitudinal vortices in the wake adversely affecting drag, flight stability and fin effectiveness [1], [2]. Streamlined fuselages with a gradual transition from main body to tail may exhibit under incidence unstable behaviour caused by alternate vortex shedding off the tail boom. Since the pressure and velocity field around the fuselage is the spatial environment in which the main and tail rotor

operate, any means to achieve flow uniformity here leads to improved aerodynamic, structural and acoustic performance [3], [4], [5].

From a formal viewpoint, the physics of these complex flows can be adequately described by the time dependent Navier-Stokes equations. If fuselage alone is considered and a time averaged flow description is aimed at, the time averaged Navier-Stokes equations together with closure equations for the turbulent stresses are needed. Due to the large computational effort involved, this approach is at present feasible only for simple basic shapes. For iterative design studies in an industrial environment, the classical inviscid flow methods coupled with boundary layer and wake modelling are favoured to provide quick decision making results at modest cost.

This paper describes the validation results of computer codes developed or in use at ONERA, Westland Helicopters Ltd., Aerospatiale and NLR to calculate the flow around a helicopter fuselage. Three fuselage configurations differing in the complexity of numerical simulation and which are typical of current generation of helicopters, were studied. All the computer codes employed are based on 3-D Panel Methods with the option to simulate boundary layer growth either by providing for an outflow over the body surface or by coupling a boundary layer code to the inviscid code. Although wake simulation option is provided in all the codes, only in one code was this option (for a rigid wake) used. With the inviscid flow pressure distribution as input, the development of boundary layer over the fuselage was evaluated with an integral and a finite difference computation scheme.

Data for the validation was provided by an extensive wind tunnel investigation with a 1:7-scale model fuselage with interchangeable rear-end. Configurations created were: a streamline model with little or no separation in its wake, an upswept rear-end model with a 'separation bubble' and strong longitudinal vortices and finally, a flat rear-end fuselage with flow separating at the periphery of the base. Rotor flow was not simulated in the theoretical and experimental investigations.

The wind tunnel model was equipped with pressure taps on body surface and rear-end. Although six component force measurements and wake surveys were also done, mainly surface pressure and rotor-plane velocity distribution was used for the code validation. Also some flow visualization, to determine the separation line on body surface was performed. Experimental data was obtained at a wind velocity of 60 m/s which corresponds to a model length based Reynolds number of four million.

2. Brief Description of the Theoretical Methods

2.1 ONERA Code and Computations

At ONERA a 3-D inviscid, incompressible steady flow code has been developed incorporating a rigid, prescribed geometry

wake [6]. The wake is modelled by a semi-infinite prismatic region with its bounding surface (vortex sheet) aligned with the onset flow. The magnitude of the velocity inside the wake, determined by a kinetic energy minimization hypothesis, turns out to be very small. Consequently the wake interior can be considered as an equipressure zone.

The total potential Φ is set as the sum of the perturbation potential of the body φ_B, wake induced potential φ_W and onset flow potential φ_∞.

$$\Phi = \varphi_\infty + \varphi_B + \varphi_W \tag{1}$$

The following formulation (see [6]) is used to determine φ_B and φ_W, Fig. 1a:

$$\begin{aligned} &\Delta\varphi_B = 0 \qquad \text{in domain } \Omega' \\ &\frac{\partial\varphi_B}{\partial n}\Big|_{\Gamma_B} = -V_\infty \cdot n \quad , \quad \text{and} \\ &\varphi_B \to 0 \qquad \text{as } |x| \to \infty \end{aligned} \tag{2}$$

And similarly

$$\begin{aligned} &\Delta\varphi_W = 0 \quad \text{in domain } \Omega', \quad \text{except on } \Gamma_W \\ &\frac{\partial\varphi_W}{\partial n}\Big|_{\Gamma_W} = 0 \quad , \quad \text{and} \\ &\varphi_W \to 0 \quad \text{as} \quad |x| \to \infty \end{aligned} \tag{3}$$

Hereby is: Δ the Laplace operator, $|_\Gamma$ the value at surface Γ, n the unit outward normal vector and $|x|$ the absolute value of the distance vector x. Solutions to equations (2) and (3) are sought so that the jump in the value of the potential φ_W across the wake surface Γ_W $(= [\varphi_W]|_{\Gamma_W})$ is such that the magnitude of velocity in the wake domain Ω_W, namely $|\nabla(\varphi_\infty + \varphi_B + \varphi_W)|$, is a minimum. A coupling of the potentials φ_B and φ_W follows from the condition that across surface Γ_W

$$[\varphi_B + \varphi_W]\Big|_{\Gamma_W} = [\varphi_W]\Big|_{\Gamma_W} \tag{4}$$

since $\quad [\varphi_B]\Big|_{\Gamma_W} = 0 \quad .$

Both the body and wake surface are discretized by a finite number of plane quadrilateral panels (see Fig. 1b*) and the procedure follows the conventional low order Panel Method approach leading to iterative solution of a system of linear algebraic equations. Velocity on the body and wake surface are

* In the actual computational model the wake surface starts from the separation line; between this line and line C the wake surface is removed in Fig. 1b to show the panelling of rear-end, which is wetted by 'dead air'.

evaluated from the resulting singularity distribution with a second order finite difference scheme. Using Green's functions, velocity in the field, e.g. in the rotor-plane, can also be evaluated. Newly developed Input/Output techniques and iterative solvers for CRAY XMP computer [7] were employed for the computations.

Only two of the studied fuselage configurations, namely the streamline and flatback, were computed using the ONERA code. For the streamline configuration little or no separation was anticipated, so that the wake model was not included in the computations. For the flatback, a wake emanating at the perimeter of the base was simulated. The line of flow separation, which can be the result of a boundary layer computation or wind tunnel experiment, needs to be known for the computations.

2.2 Westland Helicopters Ltd. Code and Computations

The method employed at Westland is based on the WBAERO code developed by AMI Inc., U.S.A.. It is a low order panel method describing steady, inviscid incompressible flow about arbitrary three dimensional bodies. A boundary layer can be simulated by adding an outflow at each panel to take account of the boundary layer growth. Other features include: wake flow modelling by emitting vortex sheets from a set of panel edges, computation of flow streamlines, evaluation of flow quantities at off-body points, etc.. Solution algorithm follows the convential steps of surface discretization and iterative solution of a system of linear algebraic equations to determine singularity strengths.

Using the WBAERO code, computation of flow around the streamline configuration was performed and rotor-plane velocities evaluated. Options of boundary layer and wake simulation were not taken in the data presented.

2.3 Aerospatiale Code and Computations

The computational approach of Aerospatiale is to evaluate the flow around the fuselage with the help of a 3-D low order Panel Method and using this as input, perform a subsequent calculation of the boundary layer growth. Aerospatiale uses for its potential flow calculations also the WBAERO code of AMI, Inc., U.S.A. without boundary layer or wake simulation.

The three dimensional boundary layer method employed by Aerospatiale is of the integral type; its code was developed by B. Aupoix and J. Cousteix at ONERA/CERT [8]. The method is based on the solution of integral equations for longitudinal and transversal momentum thickness together with an equation for the kinetic energy. Laminar and turbulent boundary layers as well as the transition laminar/turbulent can be treated. Typical results of practical interest are, the displacement and momentum thickness, skin friction coefficient and direction of skin friction lines. Boundary conditions for the code are obtained from a previous run of the Panel Method and imposed at the outer edge of the boundary layer.

The 3-D Panel code at Aerospatiale (without subsequent boundary layer computations) was used to evaluate the flow around the upswept rear-end fuselage configuration at high angle of attack and yaw. The streamline fuselage configuration, without wake simulation, was employed to study the boundary layer growth.

2.4 NLR-Boundary Layer Code and Computations

NLR contribution to the present computations consisted in evaluating boundary layer growth on the streamline fuselage configuration with the NLR three-dimensional boundary layer code BOLA, whose main features are detailed in [9] and [10]. Compressible laminar or turbulent boundary layers on arbitrary three-dimensional bodies can be computed with this method.

Based on a finite difference scheme, the method solves the equations of momentum and continuity on a general curvi-linear surface oriented mesh, whose third coordinate is taken as normal to the wall. Turbulence model employed is a simple mixing length type with a van Driest damping term.

Input to the BOLA code is the surface geometry, its curvature and derivatives as well as the pressure coefficient and its derivatives along the mesh. The pressure coefficient values used here were supplied by Aerospatiale from their panel method computations described in sec. 2.3.

3. Experimental Investigations

Wind tunnel tests were performed in the open test section of the DFVLR low speed wind tunnel in Göttingen. This facility is an open test section closed return wind tunnel with 3m x 3m cross section and a test section length of 5.86 m.

The model investigated was a 1:7 scale helicopter fuselage with interchangeable rear-ends, Fig. 2. DFVLR, MBB and Westland were involved in the conception and manufacture of the models. Front and middle part of the model remained common to all configurations. Through change of the rear part a streamline, upswept and flat back model version could be realized. The upswept rear-end model has been the subject of earlier studies [1], [2] and [11] where besides wake surveys also pressure and force measurements were conducted. Rotor flow was not simulated.

One half of the model (including the rear-end) was instrumented with pressure taps distributed over the periphery of various sections indicated in Fig. 2. The streamline model has a total of 190, the upswept rear-end model 218 and the flat back model 143 pressure taps. Scanivalves for pressure data acquisition were installed within the model.

Flow field survey in the rotor-plane was done with a ten hole directional probe which has four orifices on the conical tip arranged such as to make the pressure difference between one opposing pair sensitive primarily to incidence and the other to flow yaw. Incidence rotations are imposed until the

pressure in the opposing pair of orifices is equalized; in this condition the probe tip points nominally in the direction of local incidence. Calibration curves are used to compute the local yaw angle from the pressure difference shown by the other pair of orifices. The pressure in the central tip orifice and mean of pressures in four orifices on the cylindrical sleeve is a function of local total and static pressures respectively. Thus magnitude and direction of the local velocity vector and local pressure could be determined. The orifice on the rear-end of the probe serves to indicate flow reversal. The probe was mounted on a carriage providing remote controlled rectangular cartesian translation in the test section.

Wind tunnel tests were conducted at a wind speed of 60 m/s. The ratio of model front area to tunnel nozzle area was about 1%. Surface pressure measurements covered an angle of incidence range of $\alpha = -9°$ to $20°$ and yaw angle values $\beta = \pm 20°$. Rotor-plane velocities were measured in planes located 30 mm, 80 mm and 130 mm above fuselage upper surface. In these planes lateral traverses were done. Only streamline model was investigated.

A computerized data acquisition and reduction system enabled rapid flow field surveys. The continuously recorded probe data was integrated over 0.2 s to arrive at the average values finally recorded. Pressure measurement data was processed in a similar manner whereby values were averaged over 2 s. Choice of these integration time is based on a calibration analysis of the system.

4. Comparison of Theoretical and Experimental Results

4.1 Surface Pressure

Prediction of surface pressure with the codes employed allowed a detailed comparison with experimental results and to study the effect of flow separation and wake modelling. The good agreement between inviscid theory and experiment for low incidence and sideslip angles (in the region of attached flow) is well established. To put the code through a more severe test, a high incidence α and sideslip β angle situation (α=10°, β=15°) was chosen. The configuration studied was the upswept rear-end fuselage which is further characterized, even for low incidence, through presence of strong longitudinal vortices in its wake [11].

Panel Method results, obtained by Aerospatiale, without boundary layer and wake modelling are given in Fig. 3 for various streamwise stations*. The pressure coefficient C_p is plotted over the fuselage section contour.

In the nose region (Fig. 3a and b), the pressures on the windward side are over- and on the leeward side under predicted. Possible reasons for this discrepancy can be the low panel

* For clarity of representation different scales have been used in Figs. 3a to h.

density, development of the boundary layer, laminar separation bubbles or vortices. The boundary layer was not tripped in the experiments.

For the central part (Figs. 3c to f) the agreement between theory and experiment is good. Discrepancy on top surface, evident in Fig. 3d and e, is due to aerodynamic influence of a support strut located between these stations, which was used during experiments and not simulated in the computations.

Under side slip, the aerodynamic influence of the wake is felt more at the leeward side, as seen in Fig. 3g. Here the two sets of results differ. The experimental pressure distribution indicates through a soft peak, the presence of a vortex off the lower contour edge.

In Fig. 4a the results of ONERA computations for the streamline, and in Fig. 4b for the flat back fuselage configuration are shown. Compared is the pressure distribution on the lower surface contour in the plane of symmetry for incidence angles α of 0° and -5°. Wake modelling was provided only for the flat back configuration. The prismatic wake with a 'dead air' zone simulated in the theory is fairly representative of the real flow.

Except for a discrepancy between the results at the junction main body/tail, the results agree closely for the streamline fuselage. Slight differences in geometry of experimental and numerical model at this location are believed to be the reason. The results seem to substantiate the approach taken, that for this streamline body, the flow for the incidence range considered remains attached and wake effects can be ignored.

Fig. 4b shows the effect of wake modelling on the pressure prediciton of the flat back configuration. Both for the α = 0° and -5° case, wake simulation improves the pressure prediction, upstream and specially in the vicinity of the base. The still present deviations here are reasoned to be due to insufficient panel density employed for wake surface and the assumed wake rigidity. Aligned with onset flow of -5° incidence the lower wake surface forms a concave ramp, apparently causing the pressure rise predicted by the theory.

Pressure distributions on model surface with and without wake for α = -5° are depicted in Fig. 5. With wake simulated, the stagnation flow at the flat base is replaced by a more realistic equipressure zone.

4.2 Rotor-plane Velocity

The fuselage induced upwash and sidewash components of the velocity in the rotor-plane were computed by Westland Helicopters Ltd. and ONERA by the codes outlined in section 2.1 and 2.2. Since both approaches are based on 3-D Panel Method and the results obtained are without wake simulation, an almost identical prediction of the rotor-plane velocities was anticipated. Configuration investigated was the streamline fuselage.

Theoretical results for the upwash velocity component V_Z non-dimensionalized with the freestream velocity V_∞, are compared with experimental data of DFVLR in Fig. 6. Three rotor-plane heights are considered and data is compared at four streamwise stations as indicated. The lateral distance y is non-dimensionalized with half of maximum body width.

As indicated above, the agreement of theoretical results with each other is good. Minor discrepancies are probably due to differences in the surface discretization employed. Agreement with experimental data, except for the underpredicted values in the midregion at station x = 180 mm, is also very close.

For the same lateral and downstream stations, Fig. 7 shows the distribution of the non-dimensionalized sidewash velocity component V_Y. The experimental data shows a non-zero value of V_Y in the plane of symmetry. This is apparently a result of small errors in flow symmetry or in alignment of model/data acquisition probe. Also this set of results exhibits a very close agreement between theory and experiment.

Strong upwash and sidewash velocities exist in the windscreen area. At the farthest downstream station x = 780 mm, the fuselage tail induces a downwash and a sidewash directed towards the plane of symmetry.

The significant influence of rotor-plane height on the velocities induced is observed in the first column of the Figs. 6 and 7. The peak upwash and sidewash velocity is reduced to about one third its value for the rotor-plane height z = 458,6mm. These results illustrate the fuselage induced non-uniformity in the flow field in which the main rotor operates causing an increase in vibratory loads, noise generation and rotor power.

4.3 Boundary Layer

Extensive boundary layer computations were performed for the streamline fuselage configuration by NLR and Aerospatiale with their respective methods outlined in sections 2.3 and 2.4. Flow situation considered was zero yaw and angle of incidence $\alpha = 0°$ and $-5°$. For the sake of brevity only the negative incidence results are presented.

As mentioned earlier, the pressure distribution on the fuselage surface, which served as input for the boundary layer calculations, was that obtained by Aerospatiale from a three-dimensional Panel Method computation. The panel model presumed an attached flow over the entire body surface, so that a separation and especially its location, predicted by the boundary layer code, is subject to subsequent correction. This was, in the present excercise, not done.

The Aerospatiale code is based on an integral formulation of the boundary layer equations whereas the BOLA code of NLR utilizes a finite difference solution scheme. Accordingly the latter requires a finer computational mesh which consisted of 133 streamwise grid points and 40 grid points along the half

circumference. Each boundary layer profile was described by 41 grid points. Due to this considerable flow details were revealed.

The applicability and validity limits of both approaches are well documented in the literature and for identical input and initial conditions, similar results are obtained. Even though the input pressure distribution was identical, the point of boundary layer transition for the NLR BOLA code was set at x = 0.125 m. From this point downstream the boundary layer was considered fully turbulent. Aerospatiale calculations were performed with a free boundary layer transition from laminar to turbulent.

Fig. 8a shows the computational grid employed for the BOLA code. The computed wall streamlines from the BOLA and Aerospatiale codes are shown in Figs. 8b and c. Both methods predict a convergence of the streamlines on tail lower surface indicating the development of an 'open' separation with generation of a free vortex layer.

The iso-contours of pressure coefficient C_p on the unfolded fuselage surface, Fig. 9a, indicate low pressure regions 'A' and 'B' at the junction midbody/tail and forebody/midbody. Whereas the low pressure region A assists flow separation tendency on the tail lower surface, the region B generates a region of increased boundary layer displacement thickness (whose trace is indicated in Fig. 9b through a broken line) follows right upto the fuselage/tail junction. Also this low skin friction boundary layer flow tends to separate. These numerical results, obtained by NLR-BOLA code, suggest that through a careful modification in fuselage geometry, the low pressure regions, conducive to flow separation, can be eliminated or their occurrence delayed to higher incidence angles.

The flow in the vicinity of region A, experiences further downstream a decelaration due to tail upsweep. The resulting low skin friction boundary layer is very susceptible to existing pressure gradients in the circumferential direction. As a consequence, the wall streamlines deflect and converge as evidenced in the streamline plot of Fig. 9c.

An interesting result of the computations were the predicted drag values, which are reproduced in Table 1 below. The BOLA code of NLR indicates an increase in drag with negative incidence whereas the Aerospatiale results show a reduction which is also evident from the DFVLR experimental data. Even though NLR results are in better agreement with experiment conclusions with regard to the effect of transition (free or fixed) on forces predicted needs more substantiation. The experimental data was obtained without boundary layer tripping.

DATA SOURCE	$\alpha = 0°$	$\alpha = -5°$
	C_x	C_x
BOLA (NLR)	.003983	.003985
Cousteix (Aerospatiale)	.003590	.003530
Experiment (DFVLR)	.004500	.004400

Note: C_x, referenced to 1 m^2 (in model-scale)
$C_x > 0$: downstream along fuselage axis

Tab. 1: Drag of Streamline Fuselage

Both codes show that at low angles of attack, the drag for this configuration is predominantly friction drag, accounting for 80% to 90% of the total drag.

Effect of transition fixing can be observed in the results shown in Figs. 10 and 11. Variation of skin friction coefficient C_f along the upper and lower side of fuselage in the plane of symmetry is compared in Figs. 10a and b for the NLR and Aerospatiale computations. In Fig. 11 the C_f and displacement thickness δ^* variation over section contour at three stations is plotted.

The two sets of results are in reasonable agreement; observed differences are apparently due to the effect of the assumed location of boundary layer transition. The BOLA code, due to the finer resolution, is sensitive to small modifications in pressure gradients.

5. Conclusions

5.1 Provided no or little flow separation is present in the real flow, Panel Methods predict the surface pressure accurately. Adequate panel density in regions of flow acceleration is required.

5.2 It is demonstrated that wake simulation significantly improves the pressure prediction, specially when a region of separated flow, as at fuselage rear-end, exists.

5.3 The predicted rotor-plane velocities, induced by the streamline fuselage, agree closely with the experimental data. Strong upwash and sidewash velocities occur in the windscreen area.

5.4 The boundary layer computations show that about 80% to 90% of the total drag of the streamline fuselage stems from skin friction. Flow details identify areas on fuselage surface where geometry modification may help avoid flow separation.

Acknowledgement

The results reported represent a part of the work done under GARTEUR Action Group AG04 by the authors. Permission from GARTEUR as well as the establishments authors belong to, to publish the results is gratefully acknowledged.

References

[1] J. Amtsberg, S.R. Ahmed: "Wake characteristcs and aerodynamic forces of a helicopter fuselage", Forum Proceedings of the 9th European Rotorcraft Forum, Paper No. 4, Sept. 1983.

[2] J. Amtsberg, S.R. Ahmed: "Influence of rear end spoiler on aerodynamic characteristics and wake structure of a helicopter fuselage", Forum Proceedings of the 11th European Rotorcraft Forum, Paper No. 33, Sept. 1985.

[3] H. Huber, G. Polz: "Studies on blade-to-blade and rotor-fuselage-tail interferences", Aircraft Engineering, October 1984.

[4] J.J. Philippe, P. Roesch, A.M. Dequin, A. Cler: "Recent advances in helicopter aerodynamics". International Seminar - 'The theoretical Basis of Helicopter Technology', Nanjing, China, November 1985, ONERA T.P. 1985-166.

[5] J. Ryan, G. Falempin, T.H. Le: "Rotorplane velocities induced by a helicopter fuselage". 2nd International Conference on Basic Rotorcraft Research, College Park, Maryland, U.S.A., February 1988, ONERA T.P. 1988-22.

[6] T.H. Le, J. Ryan, G. Falempin: "Wake modelling for helicopter fuselage". 13th European Rotorcraft Forum, Arles, France, September 1987, ONERA T.P. 1987-145.

[7] J. Ryan, T.H. Le, Y. Morchoisne: "Panel code solvers". 7th GAMM Conference, Louvain, Belgium, September 1987, ONERA T.P. 1987-139.

[8] B. Aupoix, J. Cousteix: "Etude et dévelopment d'une méthode intégrale de calcul de couche limite tridimensionnelle (laminaire-turbulent) adaptée aux compresseurs". Rapport Technique ONERA 8/3327 EY 30, Sept. 1980.

[9] J.P.F. Lindhout, G. Moek, E. de Boer, B. van den Berg: "A method for the calculation of 3D boundary layers on prac-

tical wing configurations". Journal of Fluids Engineering, Vol. 103, March 1981, NLR MP 79 003 U.

[10] J.P.F. Lindhout, E. de Boer: "Manual of BOLA, description of a computational method for laminar and turbulent boundary layer flow over arbitrary surfaces". NLR TR 85087 L 1985.

[11] S.R. Ahmed, J. Amtsberg: "An experimental study of the aerodynamic characteristics of three helicopter fuselages". 13th European Rotorcraft Forum, Arles, France, September 1987.

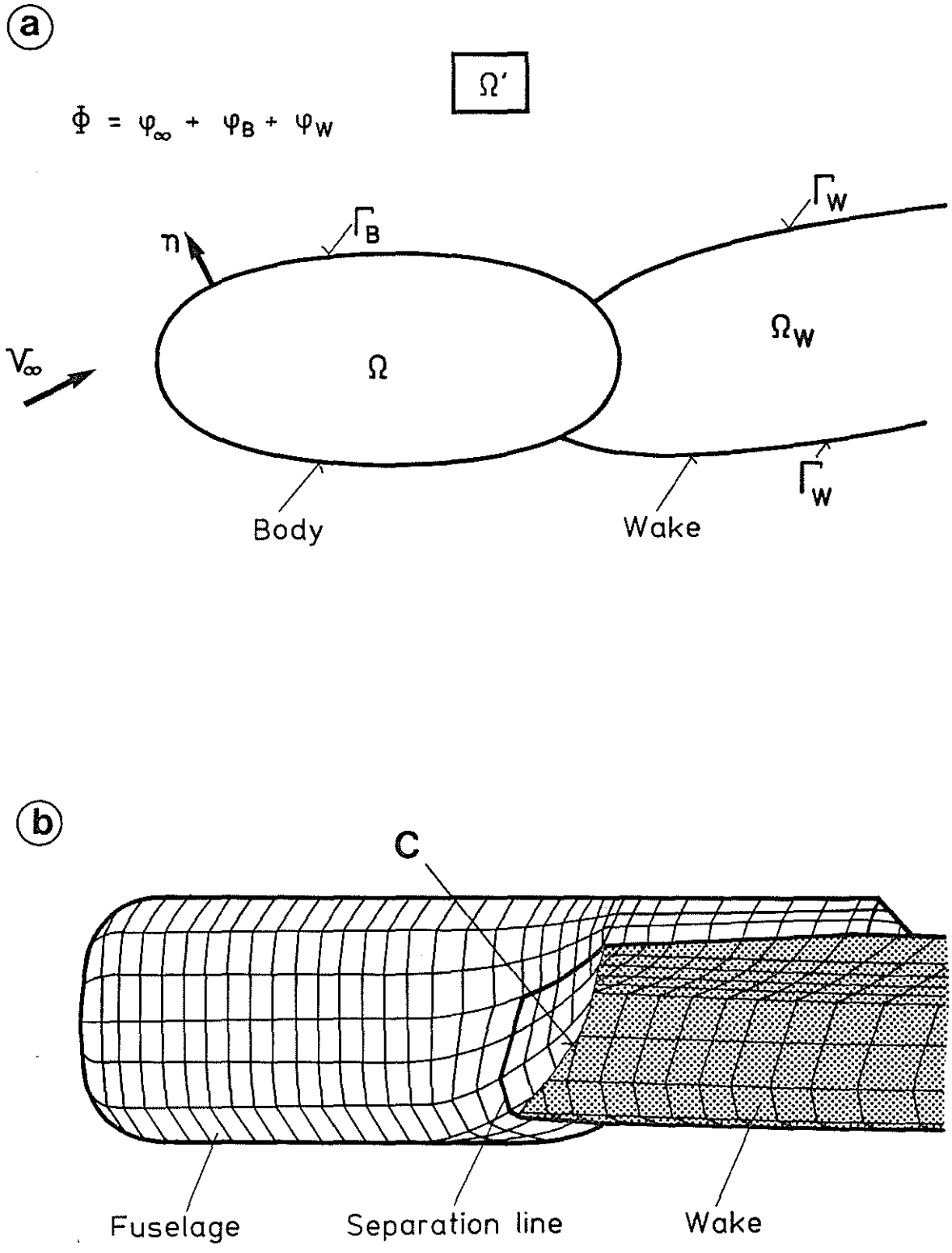

Fig. 1: a) Theoretical Formulation of Wake Model
b) Discretization of Body and Wake Surface

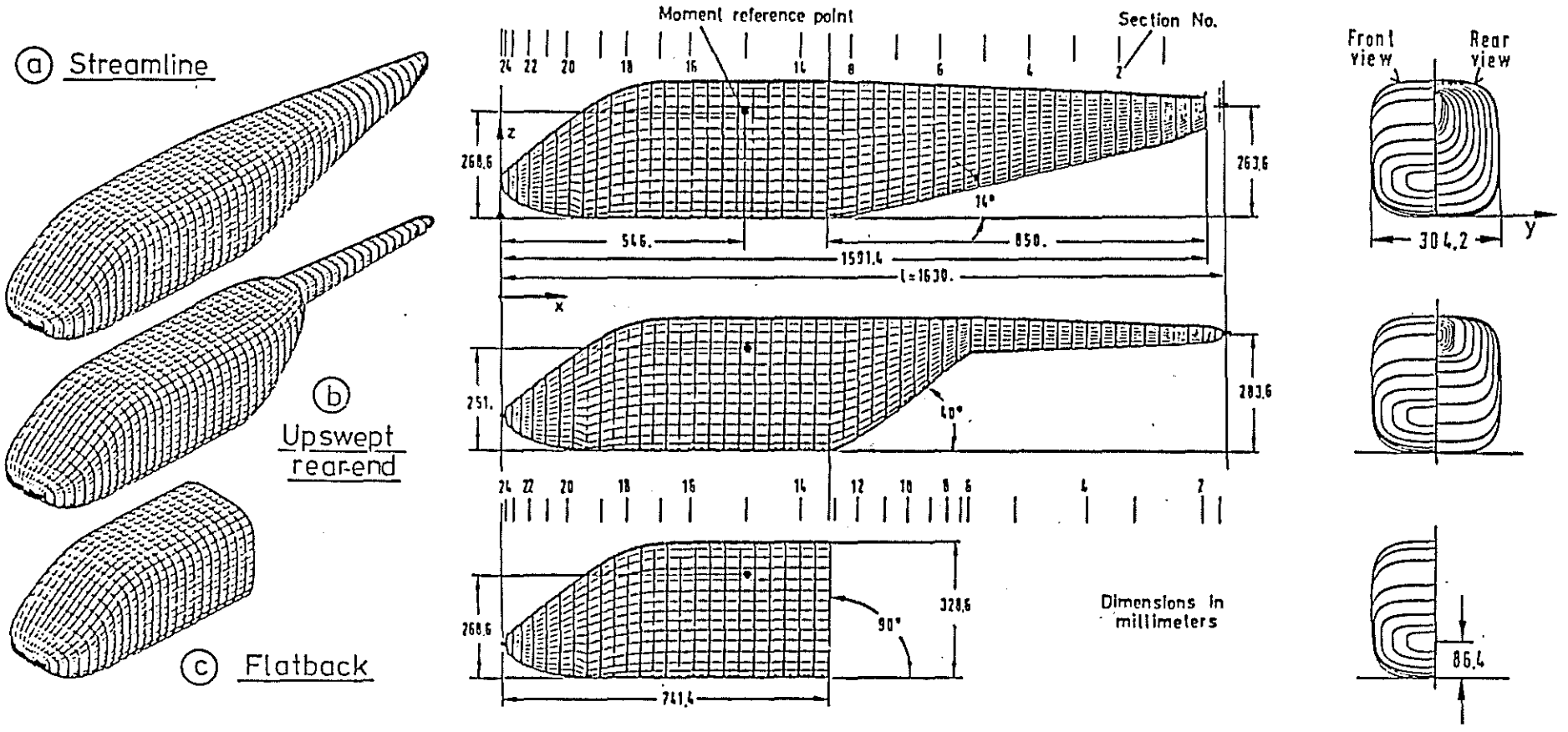

Fig. 2: Wind Tunnel Model with Interchangeable Rear-Ends

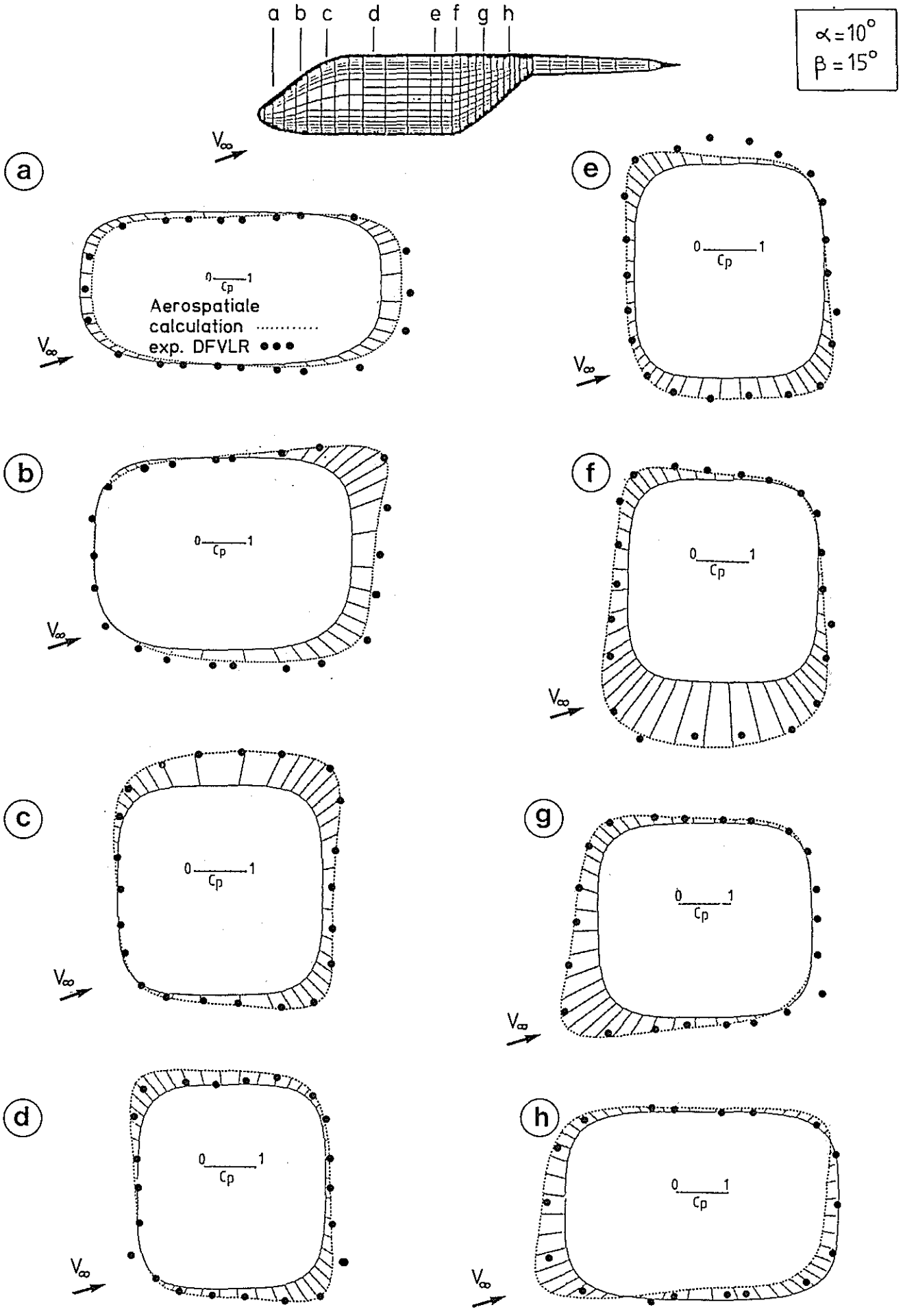

Fig. 3: Pressure Distribution on Fuselage Contour

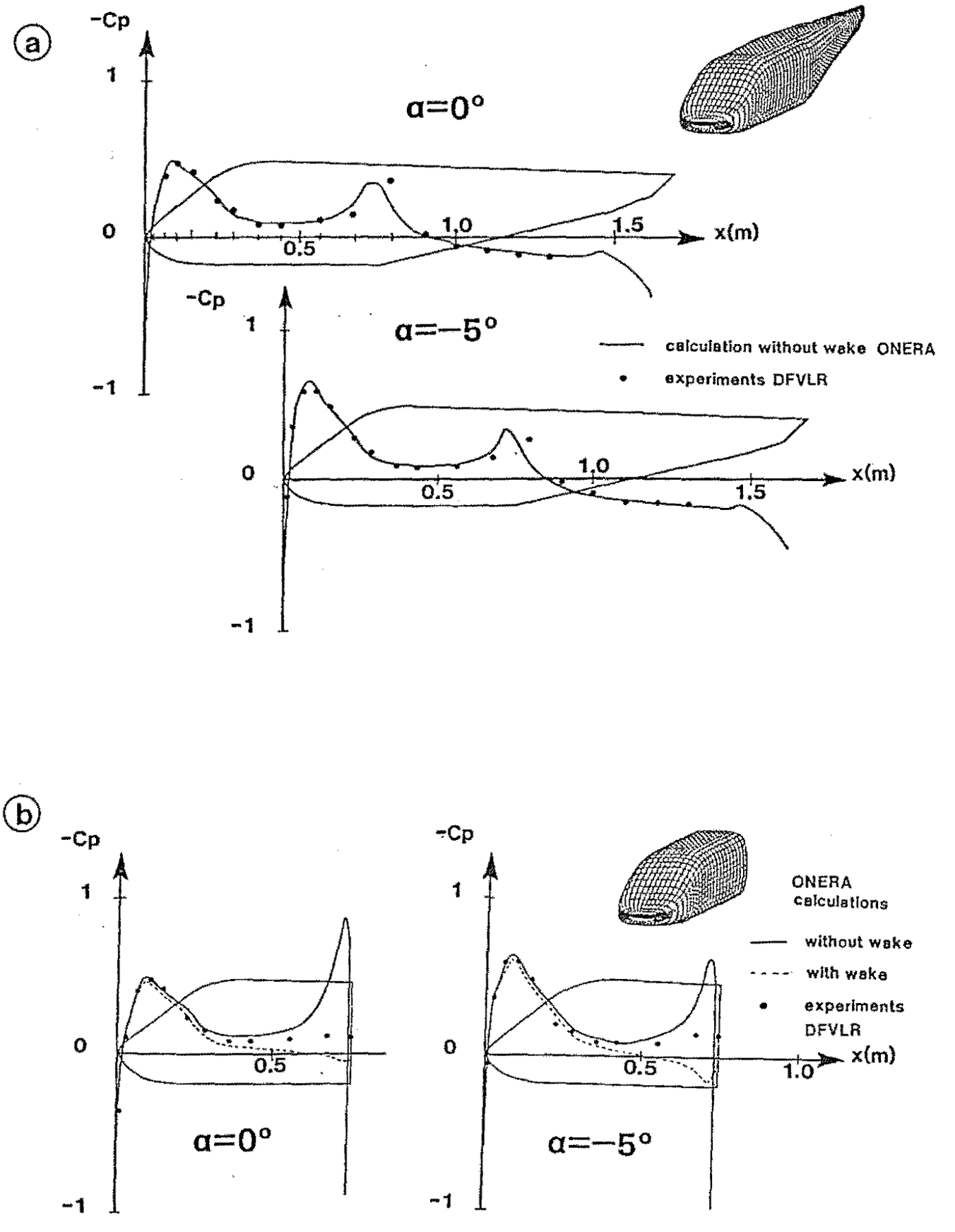

Fig. 4: Pressure Distribution along lower Surface Contour in Plane of Symmetry:
a) Streamline and b) Flatback Configuration

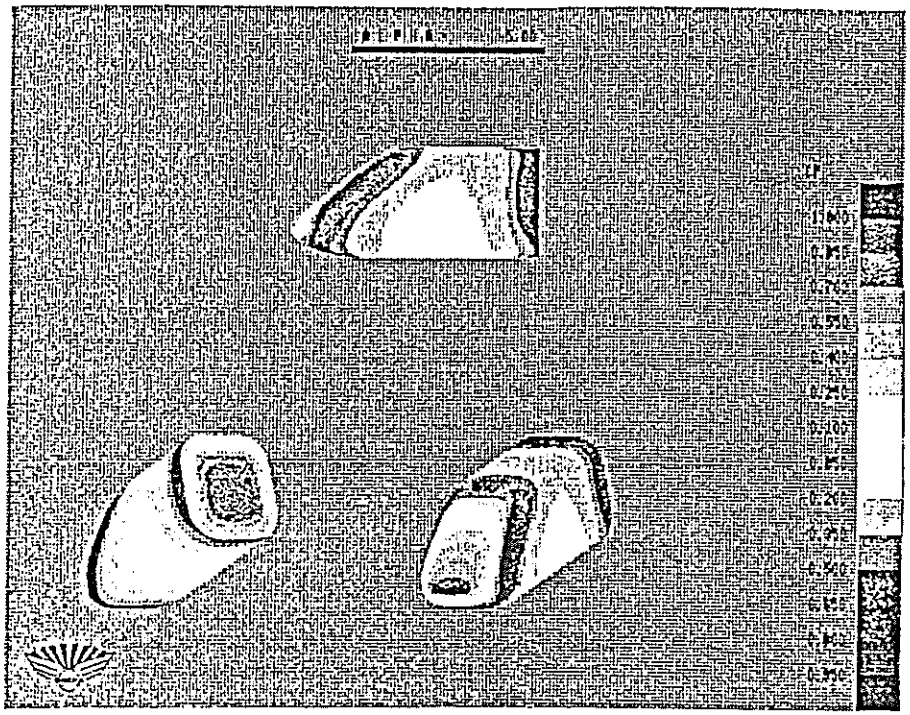

CALCULATION WITHOUT WAKE

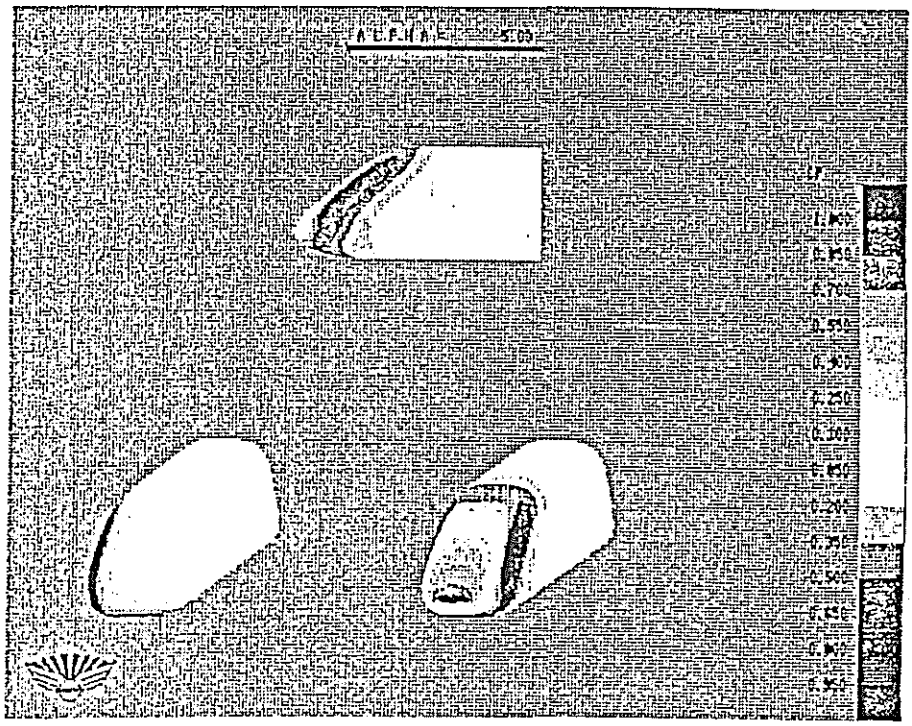

CALCULATION WITH WAKE

Fig. 5: Pressure Distribution on Model Surface.
ONERA Calculations without and with Wake

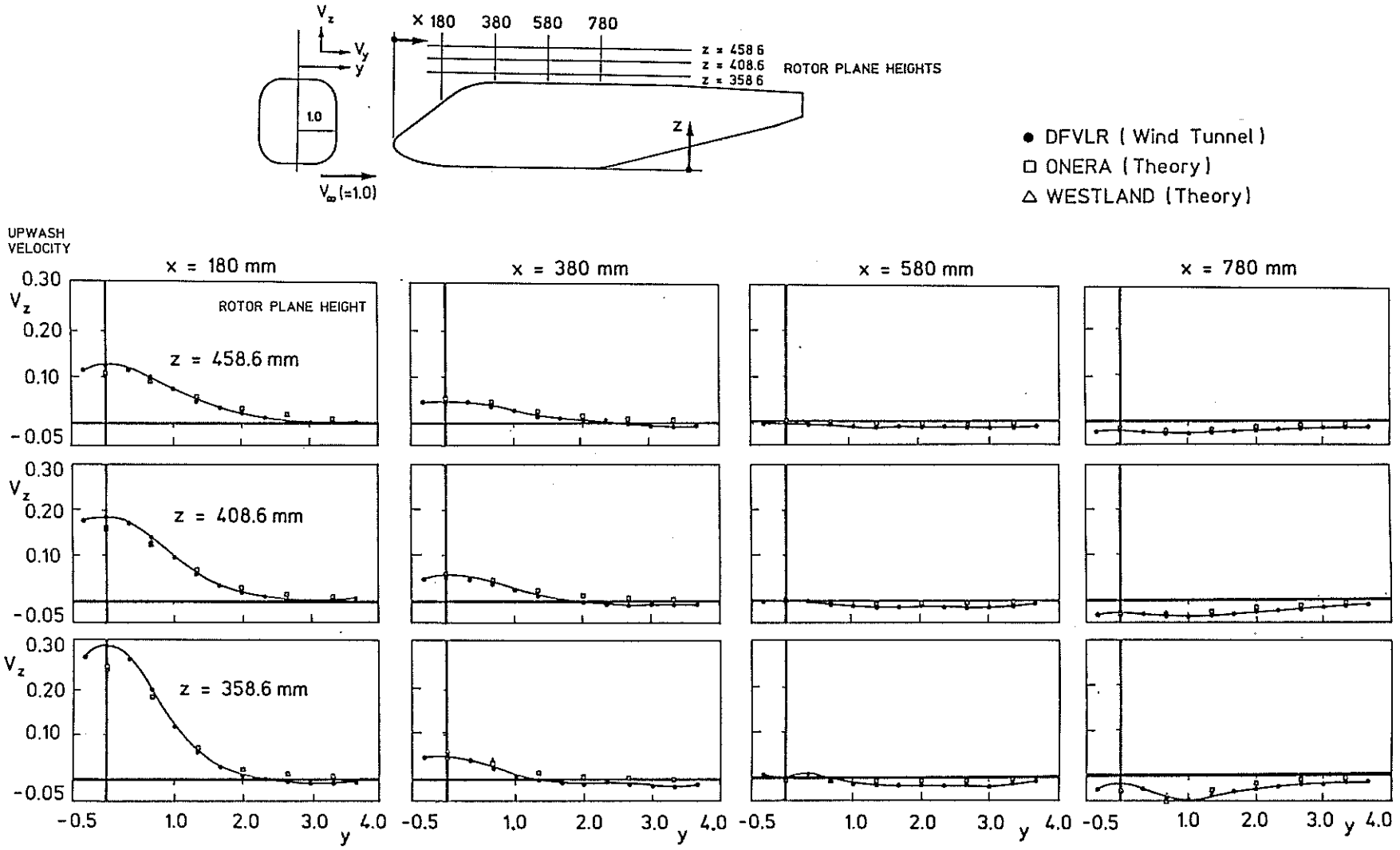

Fig. 6: Upwash Velocity in Rotor-plane

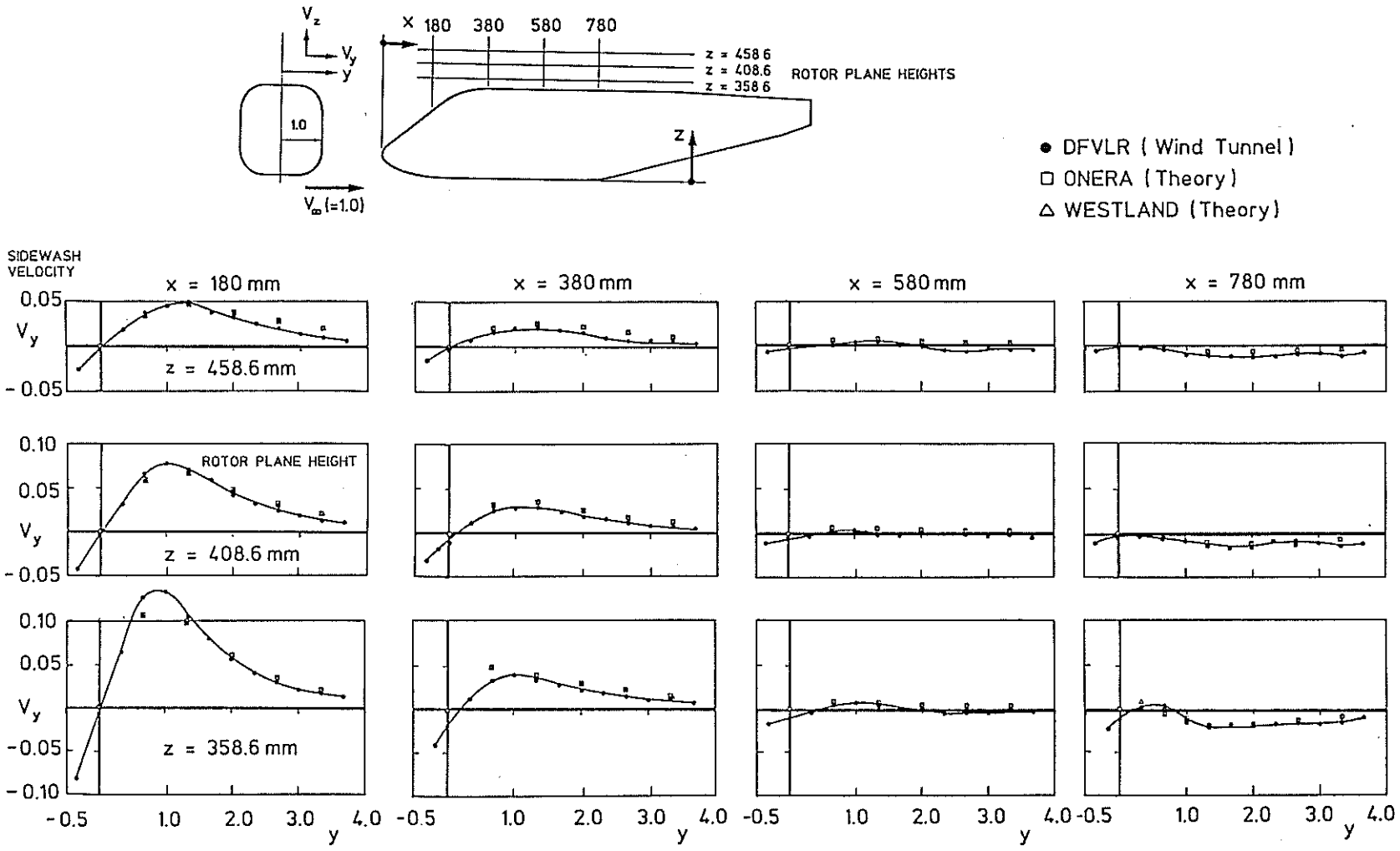

Fig. 7: Sidewash Velocity in Rotor-plane

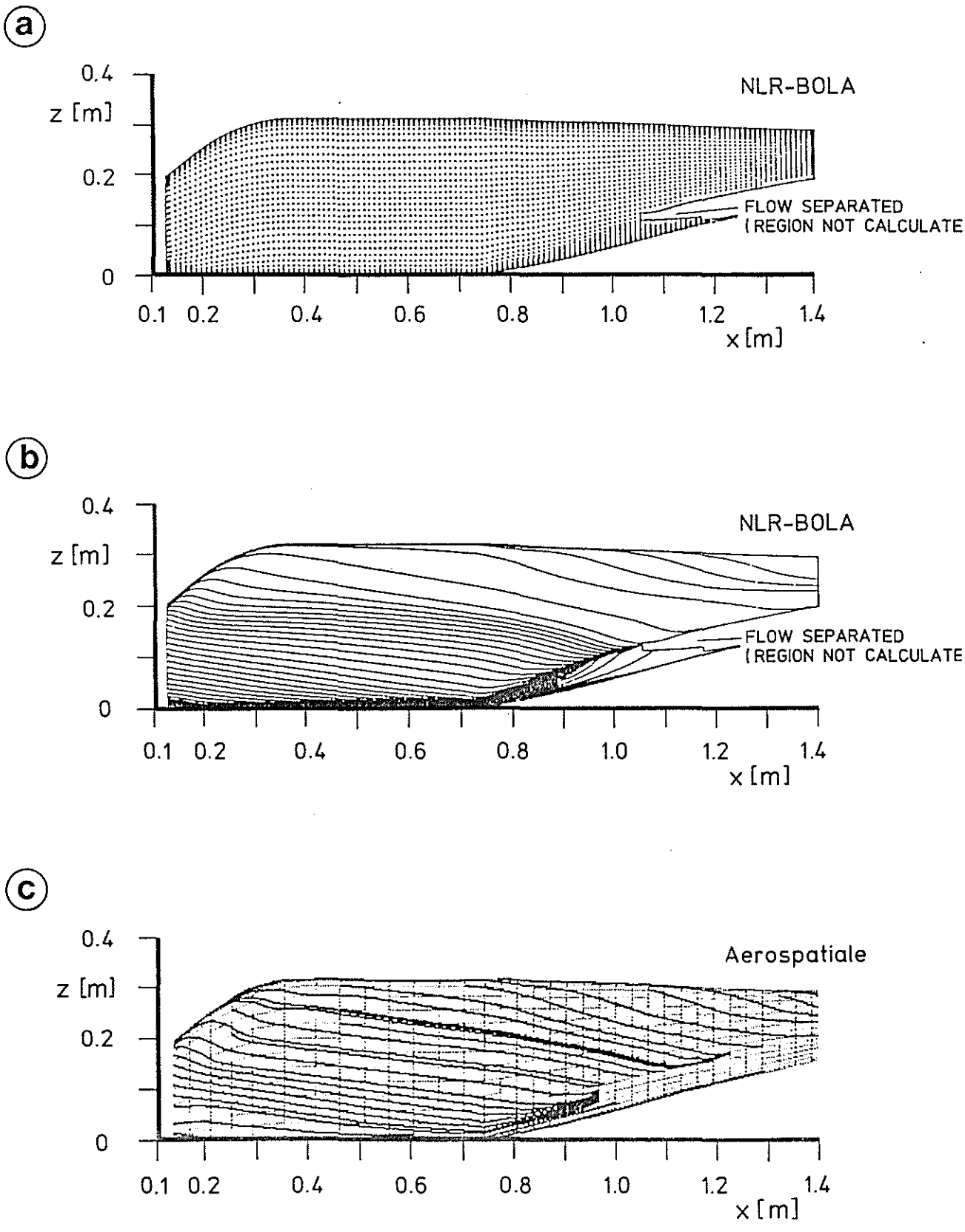

Fig. 8: a) Computational Grid for Boundary Layer Calculations

b, c) Surface Streamlines Computed with NLR and Aerospatiale Codes

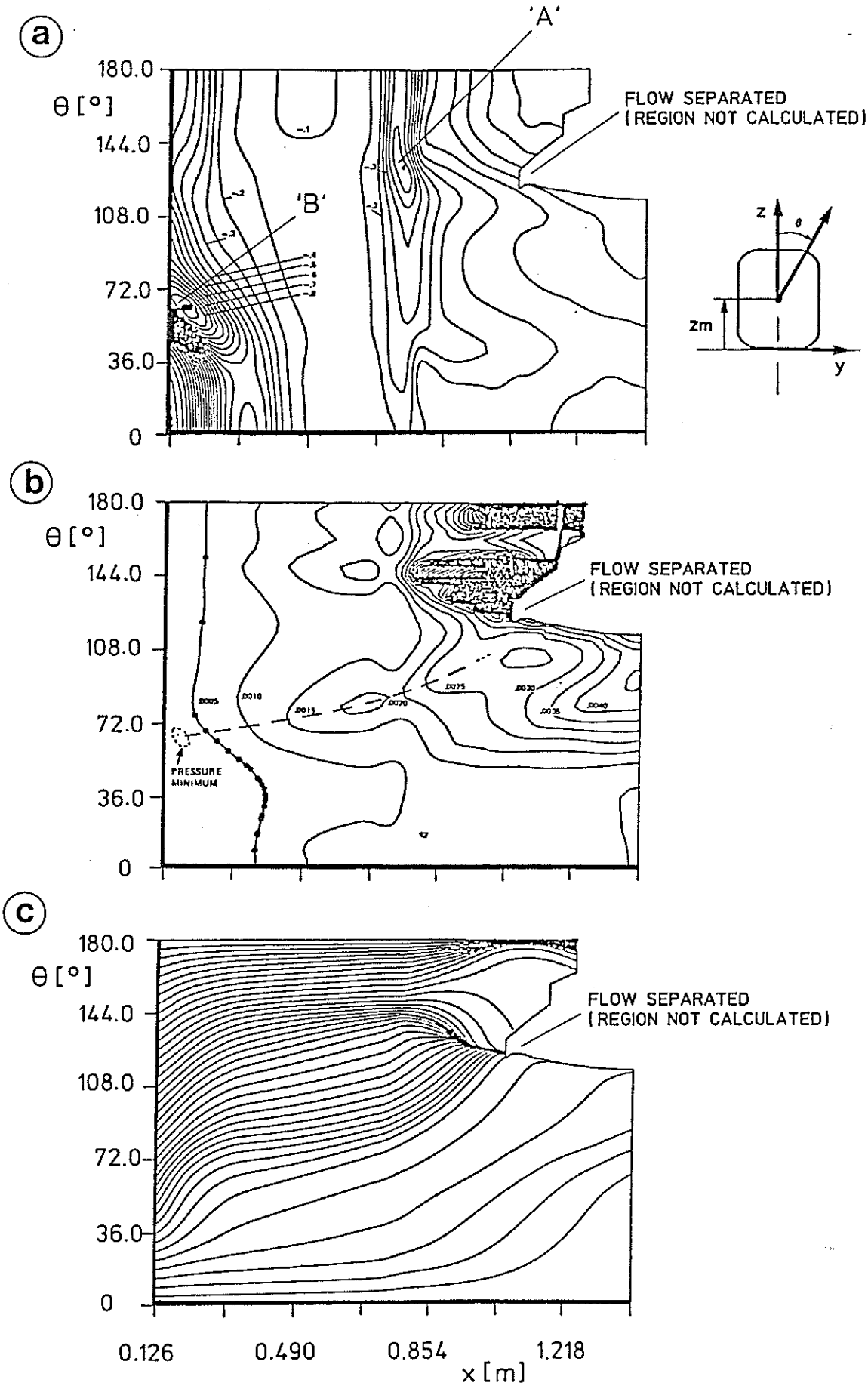

Fig. 9: a) Iso-contour Plot of Pressure Coefficient C_p

b) Iso-contour Plot of Displacement Thickness δ^* [m]

c) Computed Wall Streamline Pattern
NLR-BOLA Computations for $\alpha = -5°$

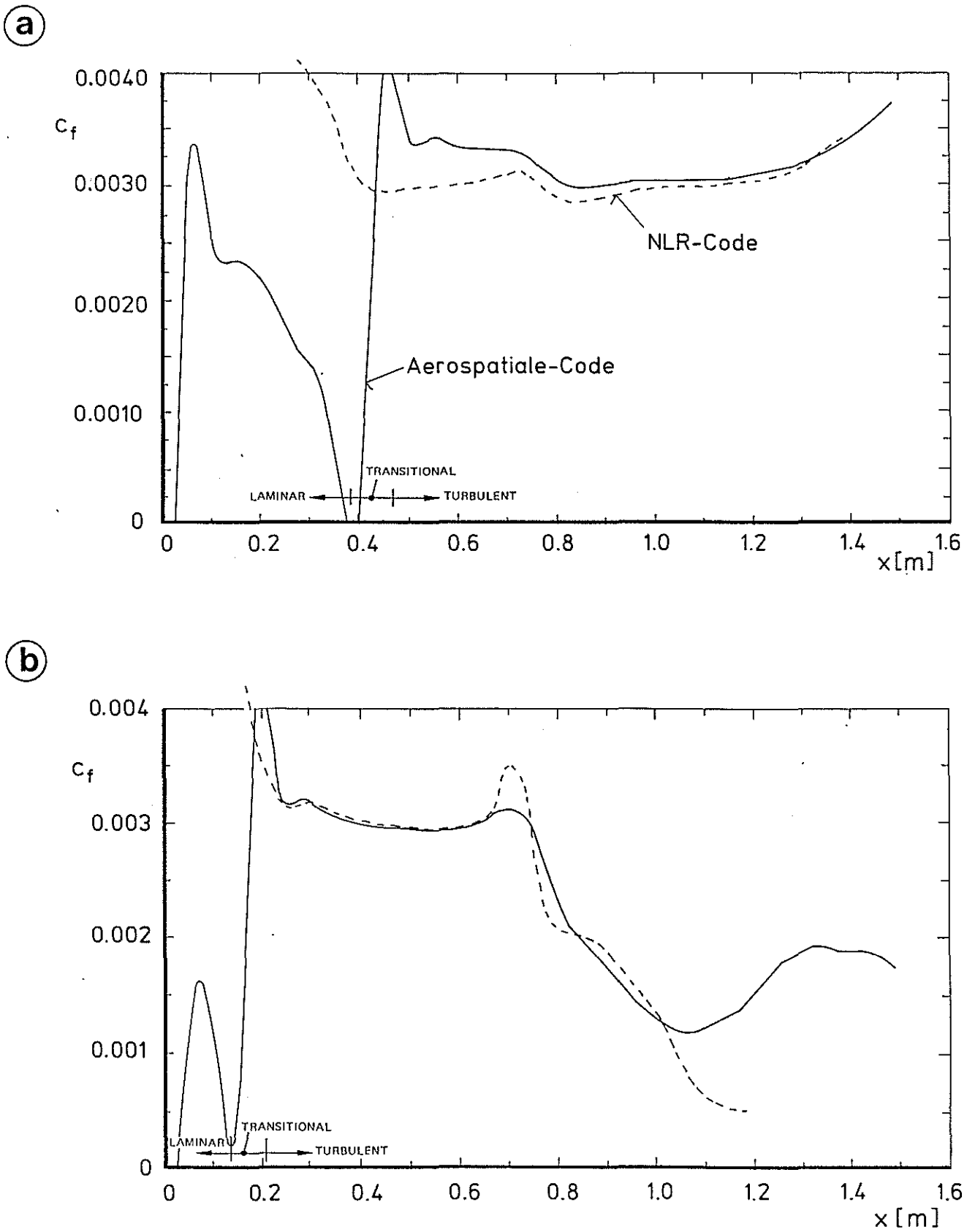

Fig. 10: Computed local Skin Friction Coefficient C_f along
a) Upper Symmetry Line and
b) Lower Symmetry Line. Streamline Fuselage, $\alpha = -5°$

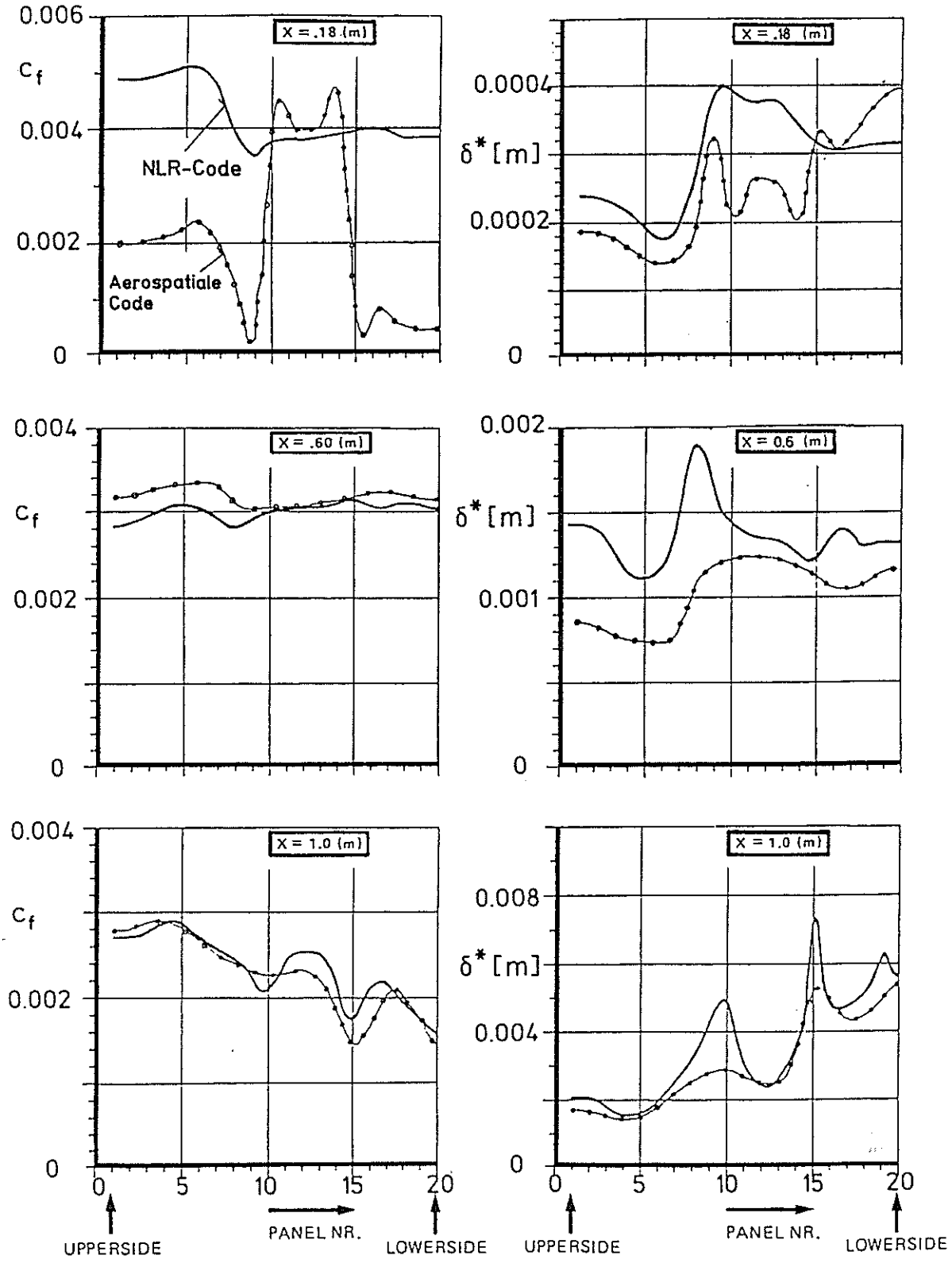

Fig. 11: Computed Skin Friction Coefficient C_f and Displacement Thickness Distribution over Contour at Various x-Stations